Large and small scales in a turbulent orifice round jet: Reynolds number effects and departures from isotropy.

G.P. Romano*

** Department of Mechanical and Aerospace Engineering, La Sapienza University, Via Eudossiana 18, 00184 Rome, Italy*

Abstract An experimental investigation of the near field of a turbulent orifice jet is performed using high resolution Particle Image Velocimetry, aiming to highlight effects on the flow field due to changes in Reynolds number. The attention is focused onto departures from isotropy for large and small scales, by considering statistics of mean square velocity and velocity derivatives and specifically the non-dimensional ratios of such quantities. The results compare well with available literature data and pointed out that the effects of Reynolds number on large scales are usually small and limited to a region ranging less than seven-ten diameters from the jet outlet. For small scales, such Reynolds number dependence is extended up to ten-fifteen diameters. Farther from the jet exit, Reynolds number dependence almost disappears and all data approach similar asymptotic behaviors. On the other hand, velocity and some velocity derivative statistics clearly show that neither large nor small scale statistics strictly follow the isotropy condition; nonetheless, differences from that condition are limited to a factor which is almost constant in the whole measured field. In order to provide a link between such large and small scale departures from isotropy, a relation among mean square velocity ratios and mean square derivative ratios is proposed and proved to be well verified in the measured region and interval of Reynolds numbers. This relation allows deriving small scale derivative ratios, which are difficult to measure experimentally or to obtain numerically, due to high resolution requirements, from large scale velocity ratios, which are achieved much easier.

**Corresponding author:* Tel.: +390644585913*;* Fax: +39 0644585250
E-mail address: giampaolo.romano@uniroma1.it

Keywords: Turbulent jet, Reynolds number dependence, Departure from isotropy, Large and small scales, PIV

Nomenclature

D	Orifice diameter
f	Longitudinal correlation function
g	Transverse correlation function
K_i	Mean square derivative ratios
K_S	Half-jet width coefficient
K_U	Jet velocity centerline decay coefficient
PIV	Acronym for Particle Image Velocimetry
R_i	Mean square velocity ratios
Re_D	Reynolds number, $Re_D = U_0 D/\nu$
Re_λ	Taylor microscale Reynolds number, $Re_\lambda = u_{rms}\, \lambda_f/\nu$
r_i	Spatial separation along i^{th} direction
RMS	Acronym for Root Mean Square
TKE	Acronym for Turbulent Kinetic Energy
U	Local mean velocity
U_0	Mean exit bulk velocity at the orifice
U_{max}	Maximum jet velocity at *vena contracta* position
u_i	Velocity i^{th} – component (u_1=u, u_2=v, u_3=w)
u'_i	Fluctuating velocity, $u_i - U_i$
u_{rms}	Streamwise velocity root mean square value
v_{rms}	Transverse velocity root mean square value
x_i	Coordinate i^{th} – component (x_1=x, x_2=y, x_3=z)
$y_{1/2}$	Half-velocity jet width
η	Kolmogorov microscale
λ_f	Longitudinal Taylor microscale
λ_g	Transverse Taylor microscale
λ_{ij}	Taylor microscale of the i^{th} velocity component along direction j^{th}
ν	Kinematic viscosity of the fluid (m^2/s)

1. Introduction and theoretical background

There is theoretical and practical broad evidence that in turbulent round jets the small flow scales behave as predicted by the axisymmetric turbulence approximation [1, 2]. Good indicators of such a small scale behavior are the mean square and mixed velocity derivatives, which retain the largest part of the Turbulent Kinetic Energy (TKE) dissipation content at high wavenumbers [3, 4]

$$\overline{\left(\frac{\partial u'_\iota}{\partial x_j}\frac{\partial u'_\iota}{\partial x_j}\right)},\ \overline{\left(\frac{\partial u'_\iota}{\partial x_j}\frac{\partial u'_j}{\partial x_\iota}\right)} \quad for\ i=1,3\ \ and\ \ j=1,3$$

(where the overbar indicates average). In order to verify simplified hypothesis, it is useful to define mean square derivatives ratios, explicitly written as eight mean square derivative ratios and three mixed derivative ratios, assuming direction 1 as main streamwise reference and 2, 3 along orthogonal axis

$$K_1=\frac{\overline{\left(\frac{\partial u'_2}{\partial x_2}\right)^2}}{\overline{\left(\frac{\partial u'_1}{\partial x_1}\right)^2}},\quad K_2=\frac{\overline{\left(\frac{\partial u'_3}{\partial x_3}\right)^2}}{\overline{\left(\frac{\partial u'_1}{\partial x_1}\right)^2}},\quad K_3=\frac{\overline{\left(\frac{\partial u'_1}{\partial x_2}\right)^2}}{\overline{\left(\frac{\partial u'_1}{\partial x_1}\right)^2}},\quad K_4=\frac{\overline{\left(\frac{\partial u'_2}{\partial x_1}\right)^2}}{\overline{\left(\frac{\partial u'_1}{\partial x_1}\right)^2}},\quad K_5=\frac{\overline{\left(\frac{\partial u'_1}{\partial x_3}\right)^2}}{\overline{\left(\frac{\partial u'_1}{\partial x_1}\right)^2}},\quad K_6=\frac{\overline{\left(\frac{\partial u'_3}{\partial x_1}\right)^2}}{\overline{\left(\frac{\partial u'_1}{\partial x_1}\right)^2}}$$

$$K_7=\frac{\overline{\left(\frac{\partial u'_2}{\partial x_3}\right)^2}}{\overline{\left(\frac{\partial u'_1}{\partial x_1}\right)^2}},\quad K_8=\frac{\overline{\left(\frac{\partial u'_3}{\partial x_2}\right)^2}}{\overline{\left(\frac{\partial u'_1}{\partial x_1}\right)^2}},\quad K_9=\frac{\overline{\left(\frac{\partial u'_1}{\partial x_2}\right)\left(\frac{\partial u'_2}{\partial x_1}\right)}}{\overline{\left(\frac{\partial u'_1}{\partial x_1}\right)^2}},\quad K_{10}=\frac{\overline{\left(\frac{\partial u'_1}{\partial x_3}\right)\left(\frac{\partial u'_3}{\partial x_1}\right)}}{\overline{\left(\frac{\partial u'_1}{\partial x_1}\right)^2}},\quad K_{11}=\frac{\overline{\left(\frac{\partial u'_2}{\partial x_3}\right)\left(\frac{\partial u'_3}{\partial x_2}\right)}}{\overline{\left(\frac{\partial u'_1}{\partial x_1}\right)^2}}$$

In particular, in axisymmetric turbulence, all mean square derivatives can be derived by only four, as reported in the following relations [2]

$$K_1 = K_2,\quad K_3 = K_5,\quad K_4 = K_6,\quad K_7 = K_8$$

$$K_9 = K_{10} = -0.5,$$

$$K_1 = (1+K_7)/3,\quad K_{11} = (1-2K_7)/6,$$

However, these specific relations do not allow evaluating the exact values of most of derivative ratios previously introduced. On the other hand, by assuming the much stronger hypothesis of isotropic turbulence, the invariance to axis direction leads to the following exact values for each derivative ratio [5]

$$K_1 = 1, \quad K_2 = 1,$$

$$K_3 = K_4 = K_5 = K_6 = K_7 = K_8 = 2,$$

$$K_9 = K_{10} = K_{11} = -0.5,$$

However such a hypothesis is hardly verified in most of interesting flows and particularly in the near field of a turbulent jet [6], thus it would be highly desirable to determine specific values for such ratios to be used as references and how they are dependent on specific conditions, as inlet and boundary conditions and Reynolds number.

The simultaneous picture from the point of view of large scales, is given by the behavior of the mean square velocity fluctuations, which retain the largest part of the TKE content at small wavenumbers [3, 4]. In isotropic turbulence, the following ratios

$$R_1 = \overline{u'^2_2} \Big/ \overline{u'^2_1}, \quad R_2 = \overline{u'^2_3} \Big/ \overline{u'^2_1}$$

must be all equal to unity. On the other hand, in axisymmetric turbulence, it is only possible to establish the equivalence of the mean square velocity fluctuations along the directions orthogonal to the mean flow, so that $R_1 = R_2$, so far the specific values once more being undetermined.

Despite the lack of theoretical and analytical support, numerical simulations and experiments on different jets allowed to obtain ranges of values for the previously defined derivative and velocity ratios [7, 8, 9, 10, 11, 12, 13, 14, 15]. For example, for those most frequently measured values, at the jet centerline, at an axial distance larger than 5 jet diameters, it is obtained

$K_1 \sim 0.7 \div 1.1$

$K_3 \sim 1.7 \div 2.1$

$K_4 \sim 1 \div 1.5$

$K_9 \sim -0.5 \div -0.3$

$R_1 \sim 0.5 \div 0.7$

$R_2 \sim R_1$

It is clearly noticed that, while some of such values, especially those related to small scales, are close to the isotropic values (K_1, K_3, K_9), others, related to both large and small scales, are far from isotropy (R_1, K_4). Such a behavior seems almost independent of the specific conditions used by the cited authors, as inlet condition and Reynolds number. The reason for this behavior is unknown, but it is surely noticeable that the ratio K_4 is the only one among those reported above, containing mean square derivatives computed only along the streamwise direction. In some sense, such streamwise mean square derivatives should be dominated by transport, that is a phenomenon acting mostly on large scales (as for R_1), whereas numerators in K_1 and K_3 are computed along the vertical direction, so far they should be definitely dominated by diffusion effects, *i.e.* by small scales. The large scales affecting transport will be typically anisotropic in the near field of a jet, while diffusion phenomena could approach more closely isotropy even near to the jet inlet. Therefore, it would be important to clarify if this picture really takes place, by also recalling theoretical relation between the previous values, especially from the point of view of relating small scales (*i.e.* K ratios) with large scales (*i.e.* R ratios).

In order to do that, we have to reconsider the way in which the mean square derivative ratios are derived. The first step is to define the longitudinal correlation functions and its Taylor expansion close to zero separation, with the hypothesis of homogeneous flow field, valid up to third-order [3, 16, 17]

$$f_{ii}(r_i \to 0) = \overline{u'_\iota(x_\iota)u'_\iota(x_\iota + r_\iota)} \cong \overline{u'^2_\iota} - \overline{\left(\frac{\partial u'_\iota}{\partial x_\iota}\right)^2}_0 \frac{r_i^2}{2} = \overline{u'^2_\iota}\left(1 - \frac{r_i^2}{\lambda_{ii}^2}\right)$$

where *i*=1 or 2 or 3. This relation defines the longitudinal Taylor microscales,

$$\lambda_{ii}^2 = \frac{2\overline{u'^2_\iota}}{\overline{\left(\frac{\partial u'_\iota}{\partial x_\iota}\right)^2}_0}$$

so that each diagonal mean square derivative can be expressed as

$$\overline{\left(\frac{\partial u'_\iota}{\partial x_\iota}\right)^2}_0 = -\left(\frac{\partial^2 f_{ii}}{\partial r_i^2}\right)_0 = \frac{2\overline{u'^2_\iota}}{\lambda_{ii}^2}$$

Similarly, it is possible to proceed for the transverse correlation functions

$$g_{ij}(r_j \to 0) = \overline{u'_\iota(x_j)u'_\iota(x_j + r_j)} \cong \overline{u'^2_\iota} - \overline{\left(\frac{\partial u'_\iota}{\partial x_j}\right)^2}_0 \frac{r_j^2}{2} = \overline{u'^2_\iota}\left(1 - \frac{r_j^2}{\lambda_{ij}^2}\right)$$

where $i \neq j$, allowing to define the transverse Taylor microscales,

$$\lambda_{ij}^2 = \frac{2\overline{u'^2_\iota}}{\overline{\left(\frac{\partial u'_\iota}{\partial x_j}\right)^2}_0}$$

so that again cross mean square derivatives can be expressed as

$$\overline{\left(\frac{\partial u'_\iota}{\partial x_j}\right)^2}_0 = -\left(\frac{\partial^2 g_{ij}}{\partial r_j^2}\right)_0 = \frac{2\overline{u'^2_\iota}}{\lambda_{ij}^2}$$

Now, if isotropy is assumed, the second-order derivatives of f and g will not depend on the specific direction r_i, (i=1, 2 or 3), so that immediately some exact relation can be derived for the mean square derivative ratios

$$K_1 = K_2 = 1,$$

$$K_3 = K_4 = K_5 = K_6 = K_7 = K_8$$

and of course for the Taylor microscales

$$\lambda_{ii} = \lambda_f$$

$$\lambda_{ij} = \lambda_g$$

However most of the previous ratios are still not determined, unless a specific relation is established among the longitudinal and transverse correlation function. This can be derived by using the hypothesis of incompressible flow, which therefore is an additional hypothesis [3, 16, 17]

$$f + \frac{r}{2}\frac{\partial f}{\partial r} = g$$

also implying

$$2\left(\frac{\partial^2 f}{\partial r^2}\right)_0 = \left(\frac{\partial^2 g}{\partial r^2}\right)_0$$

and

$$2\lambda_g = \lambda_f$$

Thus, in addition to the previous ratios, it is possible to derive

$$K_3 = K_4 = K_5 = K_6 = K_7 = K_8 = 2$$

Furthermore, additional relations among small and large scale ratios are here derived, by considering the plane containing axial and transverse directions (1, 2), the first one from the definition of Taylor microscales λ_{21} and λ_{11},

$$K_4 = 2\,R_1/A$$

where A is a non-dimensional factor almost equal to 1, deriving from the specific relation among the squares of λ_{21} and λ_{12}, in case of departure from isotropy. The second one is cross-relation from the other Taylor microscales definitions on the same plane (1, 2)

$$K_3 / K_1 = 2A / R_1$$

Similar relations can be obtained in the other coordinate planes, as for example $K_6 = 2R_2/B$ (where B is again a non-dimensional factor almost equal to 1, deriving from the specific relation among the squares of λ_{31} and λ_{13} in case of departure from isotropy).

The previous relations, and in particular the one between K_4 and R_1, not only gives a way to relate small and large scales and their departures from isotropy, but also allows to derive an estimation of mean square derivatives on small scales as K_4 (which suffer from high resolution requirements both numerically and experimentally), from the measurement of mean square velocities on large scales, as R_1, which can be derived much more easily.

Therefore, moving from these relations, the first aim of this paper is to determine experimentally, using high resolution Particle Image Velocimetry (PIV), the mean square velocities and mean square derivatives in the near field of a turbulent jet, in order to verify the above reported relations, by comparing direct measurements of K ratios with estimates using the R ratios. The second objective of this work, is to verify the dependence of velocity and velocity derivatives on specific inlet conditions, in terms of dynamical actions, *i.e.* on Reynolds number, with the specific goal of revealing departures and approaches to isotropic conditions.

2. Experimental facility and measurement technique

A sketch of the experimental setup is presented in Figure 1, the circular nozzle being produced with a sharp edge contour, with roundness less than 0.5 mm, thus ensuring proper developing of the shear layers. The nozzle is manufactured on a plate, so that the jet can be considered as an orifice jet, the plate dimensions on the coordinate planes (x_1-x_2 and x_2-x_3, x_1=x being the streamwise direction and x_2=y and x_3=z the vertical and transverse ones) being around 20 D (where D=2cm is the diameter of the orifice).

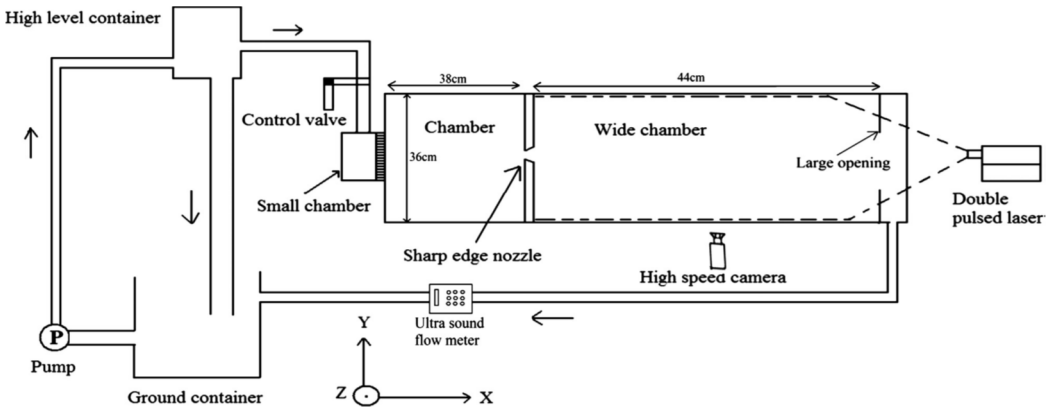

Figure 1. Schematic view of the experimental setup, the flow direction in the test section is from left to right.

As shown in Figure 1, the continuous jet is part of a closed loop hydraulic circuit starting from a ground container, from where a centrifugal pump moves water to a high level container (around 4 meters in height, which can be adjusted to change the jet velocity), to smooth fluctuations due to the pump. Once flowed out from such a tank, the water enters through a small chamber and honeycombs into the test tank, which is subdivided by the orifice plate into a settling chamber (38 cm in size, about 18 D, upstream of the orifice) and the proper test chamber (58 cm, about 30 D, downstream the orifice). Finally, a second plate delimits a discharge chamber, downstream to the test one, through which the water comes back to the main tank, so far closing the loop. The whole test section is made by Plexiglas to allow optical access. The flow rate is measured

by an ultrasound flow meter, placed between the discharge chamber and the ground container, with an error of ±2.5%.

Dynamical conditions are determined mainly by the Reynolds number defined by $Re_D = U_0 D/\nu$ (where U_0 is the exit bulk velocity, D is the diameter of the orifice, and ν the kinematic viscosity of water) set between 2,000 and 70,000. The Taylor microscale Reynolds number, defined by $Re_\lambda = u_{rms}\,\lambda/\nu$ (where u_{rms} is the streamwise *rms* velocity and λ is the longitudinal Taylor microscale), is between 80 and 500. For $Re_D = 1.5\times10^4$, it is obtained $\lambda = 2.1\times10^{-3}$ m and $\eta = 2.2\times10^{-4}$ m for the Kolmogorov length scale, derived by employing the Kolmogorov local isotropy hypothesis to derive an estimate of the TKE dissipation.

The present experimental study has been carried out by means of Particle Image Velocimetry technique. The acquisition system is composed of a light source, namely a double-pulse Nd-Yag laser having 200 mJ energy per pulse, forming a light plane with around 1 mm thickness and a minimum pulse duration of 8 ns, and an acquisition device, *i.e.* a digital high-speed camera (2,000 frames/s at maximum resolution), with 1,024 × 1,024 pixel resolution and a 10 bit CMOS sensor. Between them, a BNC 575 pulse generator allows the synchronization between laser illumination and camera recording. The camera had a 17 μm sensor pixel size, a 50 mm focal length objective, with an aperture equal to F = 1.8 and a working distance near to 20 cm, due to an extension tube set. The attention is focused on to the near jet region, *i.e.* $x/D < 25$ for two main reasons: primarily, earliest investigations revealed that all large and small scale statistics are basically independent on Reynolds number for $x/D > 25$. In addition, the majority of interest for engineering applications is related to the near field, where different strategies (change in geometry, Reynolds number and active solutions) can be applied to improve mixing and convergence to isotropy conditions as also related to numerical approximations. In order to improve the spatial resolution of the measurements, the acquired near jet region is divided into sub-regions, each one by 3.5 D, imaged at full camera resolution, *i.e.* with a resolution around 130 pixel/cm. Details on the dependence of results on image resolution are reported in [6]. The water was seeded by glass hollow beads having a diameter in the range (8 – 12) μm and a density around (1.05−1.15) g/cm^3, the particle image size being in between (1.5 - 2.3) pixels. Acquired images have been analysed by LaVision Davis 7 software, making use of a multi-pass algorithm consisting of two passes with a large window

size equal to 64 × 64 pixels and four passes with a smaller window of 32 × 32 pixels, in both cases using 75 % overlapping. Thus, the final spacing between velocity vectors was 8 pixels, which is equal to about 0.5 mm, *i.e.* on the average around $\lambda/4$ and 2η. In addition, a vector validation algorithm, based on a local median filter and group removing, is applied to eliminate spurious vectors. The LaVision Davis software performances in the 3rd PIV Challenge attained a bias error less than 0.5% and an *rms* error around 5%, dependent on the quality of acquired images [18]. Such a bias error is consistent with an absolute error of ±0.05 pixels (which is typical of advanced PIV processing) and an average tracer displacement of 10 pixels.

To derive statistics of velocity and velocity derivatives, for each Reynolds number, about 10,000 image pairs have been acquired in subsets of 1,000 at a repetition rate of 10 Hz, so that each acquisition took 100 s, ensuring statistical independence between samples in time. Indeed, the integral time scale is around 4 ms, which is much smaller than the repetition time of 0.1 s, so that there are 25 integral time scales between each sample in time. In addition, the total number of samples is sufficient for proper statistical convergence, as shown in a previous paper by looking at probability density function dependence on the number of samples [6]. The space derivatives have been computed by making use of finite difference approximations with second order accuracy, except at the boundaries. From this point of view, it is important to underline that in this paper only spatial derivatives are computed and that keeping the vector spacing around to two Kolmogorov scales also ensures a good evaluation of spatial velocity differences [19].

3. Results and discussion

The detailed characterization of the orifice jet has been already performed elsewhere [6, 15, 20], so hereafter the attention will be focused on the effect of Reynolds number on large and small scale statistics and on the relation among them in view of departures from isotropy as detailed in the first section of this paper.

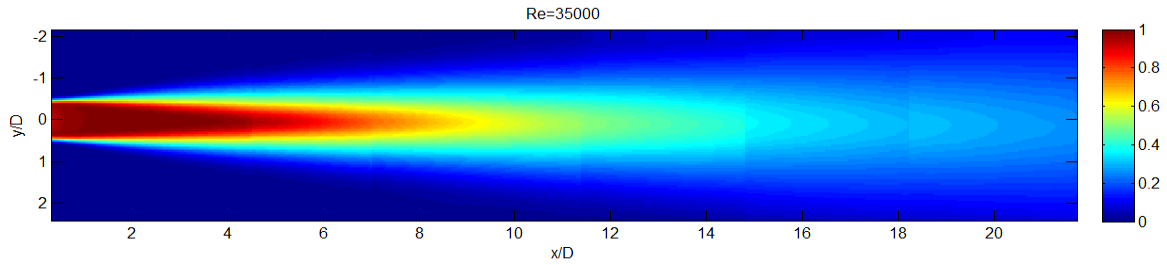

Figure 2. Colormap of normalized streamwise velocity component in the near field of the orifice jet for Reynolds number equal to 35,000. The flow direction is from left to right.

3.1. Large scale statistics

The streamwise velocity field, obtained from the data in the near jet region, is shown in Figure 2 for a Reynolds number of 35,000. The velocity is normalized with the maximum velocity, U_{max}, which for an orifice jet is not attained just at the outlet, but slightly downstream, usually at one diameter due to the *vena contracta* phenomenon [21, 15]. This is visible in Figure 2, where the exit velocity is increasing when moving downstream along the centerline, as also the usual decay of velocity and spreading of the jet in the ambient fluid after the end of the jet core, around 5*D*. In the figure, it is also possible to notice the different sub-regions used to assemble the whole jet behavior with high resolution. Similar behaviours are obtained for the flow fields at the other Reynolds numbers and to point out the effect of the latter, the inverse of the streamwise mean velocity decay along the centerline is reported in Figure 3.

From such a figure, again it is possible to notice the acceleration close to the jet orifice due to the *vena contracta*, the location for the maximum velocity (which is a minimum in this plot) being around (1-2)*D*, slightly dependent on Reynolds number. On the other hand, from around 5*D*, after the end of the jet core region, the centerline velocity starts to decay almost as 1/*x*, which is a linear behavior in this inverse decay plot

$$U_{max}/U = K_U\,(x/D) + C_U\,.$$

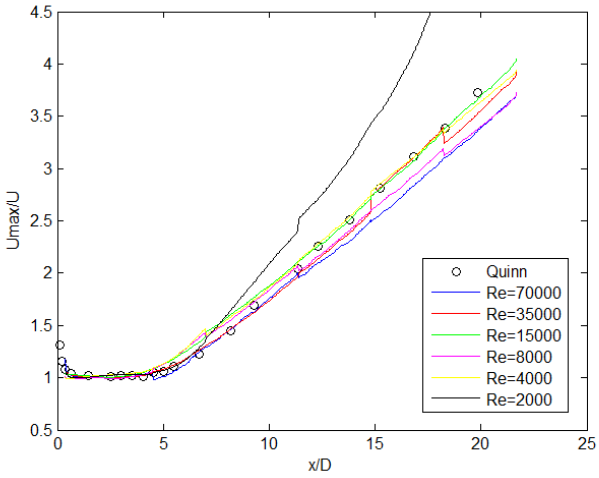

Figure 3. Inverse of mean streamwise velocity centreline decay measured at different Reynolds numbers. The black circles refer to the data reported by Quinn (1989) [22], obtained on an elliptical orifice jet at a Reynolds number almost equal to 10^5.

Only the data acquired at Re=2,000 depart from such a behavior, showing an almost non-linear trend, with a stronger centerline velocity decay in comparison to the other data. Apart from this, the overall behaviors are in agreement with data by Quinn (1989) and (2007) [22, 21], obtained by Hot Wire Anemometry on an elliptical orifice jet at a Reynolds number almost equal to 10^5, which are closely overlapped also with data by Mi *et al.* (2007) [10], obtained with PIV on a circular orifice jet at Re=70,000.

The previous reported decay coefficient K_U has been extensively investigated in the past, as also its counterpart in terms of jet half-width increase, which again results as linear within the hypothesis of jet self-similarity [23, 22]:

$$y_{1/2}/D = K_S\,(x/D) + C_S\,.$$

The behaviour of the coefficients K_U and K_S as a function of Reynolds number is reported in Figure 4, compared with results by other authors [23, 24, 25, 26]. For both, there is a decrease from small to high Reynolds numbers, reaching almost constant values, $K_U \approx 0.15$ and $K_S \approx 0.1$ respectively, in good agreement with existing data. Certainly, it is reasonable to get a smaller decrease in centreline velocity (small K_U) when the jet aperture is also small (small K_S) and this behaviour is observed for Reynolds numbers not exceeding 10^4. This means that the jet development is expected to be faster for low Reynolds number jets. On the other hand, the jet decay and spreading is slightly dependent on Reynolds number if this is larger than 10^4.

Regarding velocity fluctuations, examples of color plots for the *rms* of streamwise and radial velocity components are presented in Figure 5, as derived for a Reynolds number equal to 35,000. Again values are made non-dimensional by using the maximum velocity at the *vena contracta* section. The two developing shear layers are clearly observed, merging at about 5*D*, *i.e*. where the jet core region ends, with maximum non dimensional values of fluctuations almost equal to 0.15 and 0.1 respectively for the two components.

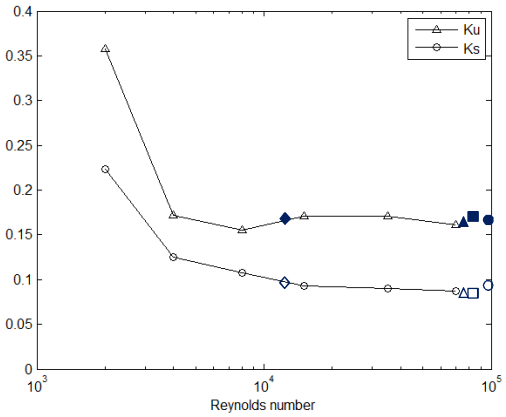

Figure 4. Jet velocity and half-width coefficients, K_U and K_S, as measured at different Reynolds numbers (symbols connected by lines). The single circles (filled for K_U and open for K_S) refer to the data reported by Quinn (2006) [24], squares to data by Wygnansky and Fiedler (1969) [23], triangles to data by Chen and Rodi (1980) [25] and diamonds to those by Panchapasekan and Lumley (1993) [26].

The present results are is good agreement with those obtained by other authors [21, 15] and similar behaviours are obtained also for the measurements at different Reynolds numbers. To this aim, in order to compare the data acquired at different Reynolds numbers, the centerline trends of the two non dimensional *rms* fluctuations are presented in Figure 6 and compared with data by Quinn (2007) [21], obtained by Hot Wire Anemometry on an elliptical orifice jet at a Reynolds number almost equal to 10^5. The first thing to notice is that the data collapse quite well for both components for *x/D* larger than around 7, whereas there is a relevant variability for smaller distances, expecially if the Reynolds number is smaller than 15,000, again showing an earlier development of low Reynolds number jets. This is proving that the local maximum jet velocity at the *vena contracta* position, used in this plot, is a good scaling reference velocity. In addition, it is confirmed that the peaks in *rms* fluctuations for both components are located in the region *x/D* between 5 and 8, with a value in the range (0.12 - 0.16) for the streamwise component and in the range (0.09 – 0.15) for the radial component.

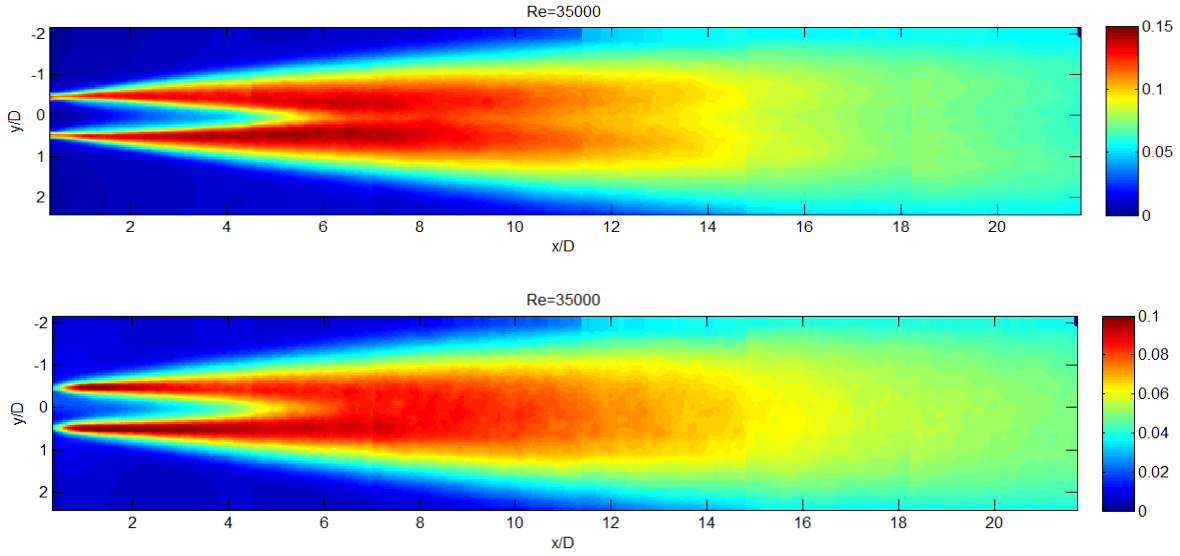

Figure 5. Colormaps of normalized *rms* fluctuations for streamwise (at the top) and radial (at the bottom) velocity components in the near field of the orifice jet for Reynolds number equal to 35,000. The flow direction is from left to right.

These results are in agreement with the reference data, obtained by Quinn (2007) [21] for similar Reynolds numbers, even if on an elliptical jet, which usually gave some slightly overestimated *rms* value [15]. An equivalent collapse of data at different Reynolds number is obtained if considering the behaviours in the shear layers or along the transverse directions (not shown here).

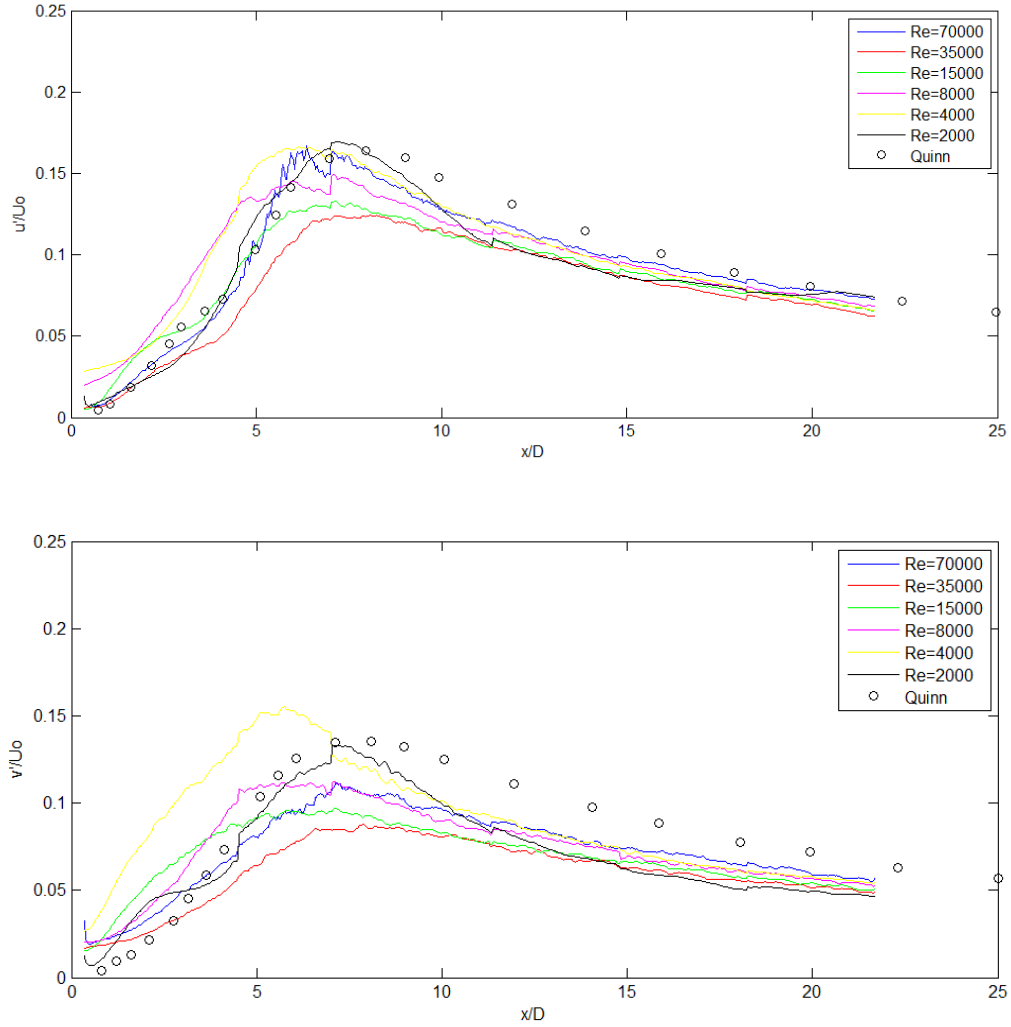

Figure 6. *Rms* fluctuations at the jet centreline for the streamwise (at the top) and radial (at the bottom) velocity components as measured at different Reynolds numbers. The black circles refer to the data reported by Quinn (2007) [21], obtained on an elliptical orifice jet at a Reynolds number almost equal to 10^5.

From these *rms* fluctuations, it is possible to derive the ratio among mean square velocity variations along two orthogonal axes, *i.e.* u_{rms}/v_{rms}, which is not dependent on the specific velocity used to have non-dimensional quantities, so quite a general properties of the considered flow. A color plot example is presented in Figure 7, for a Reynolds number equal to 35,000. This ratio is also equal to the inverse of the root of the invariant R_1 introduced in section 1 of this paper, so that a value equal to 1 is expected for fully isotropic conditions on large scales. Indeed, the result reported in Figure 7 points out that, apart from the external ambient fluid, starting from shear layers, an almost constant value spreads all over the field, as indicated by the dominant green-yellow colors. Noticeable is the fact that this color is different from the one related to the value 1, which is light blue. This consideration can be made more quantitative by considering the centerline profile of this ratio, for the different Reynolds numbers tested, as reported in Figure 8. In the first 5 diameters there are strong variations at the different Reynolds numbers, which are replicating the differences observed in mean and *rms* velocities due to large scale vortices, whereas for $x/D>7$, the data are well grouped and close to the results reported as references, except possibly for the very small Reynolds number. They reach an almost constant value, which as already noted is different form unity, lying in the interval (1.2 – 1.4), in agreement with the interval (0.5 – 0.7) reported in the Introduction of this paper for the quantity R_1.

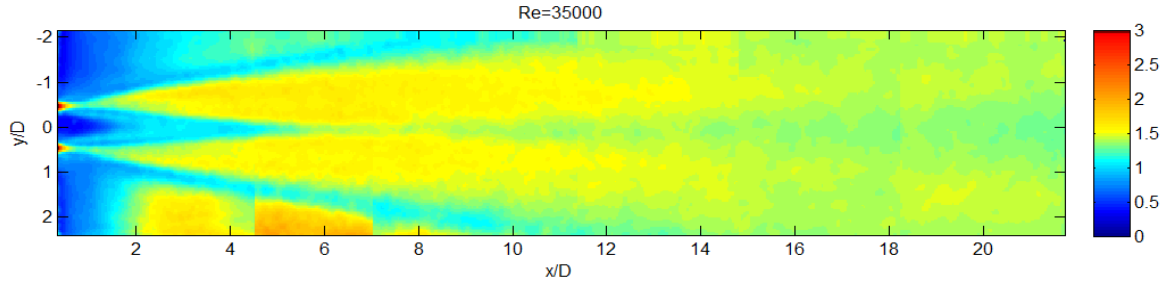

Figure 7. Colormap of the ratio u_{rms}/v_{rms} in the near field of the orifice jet for Reynolds number equal to 35,000. The flow direction is from left to right.

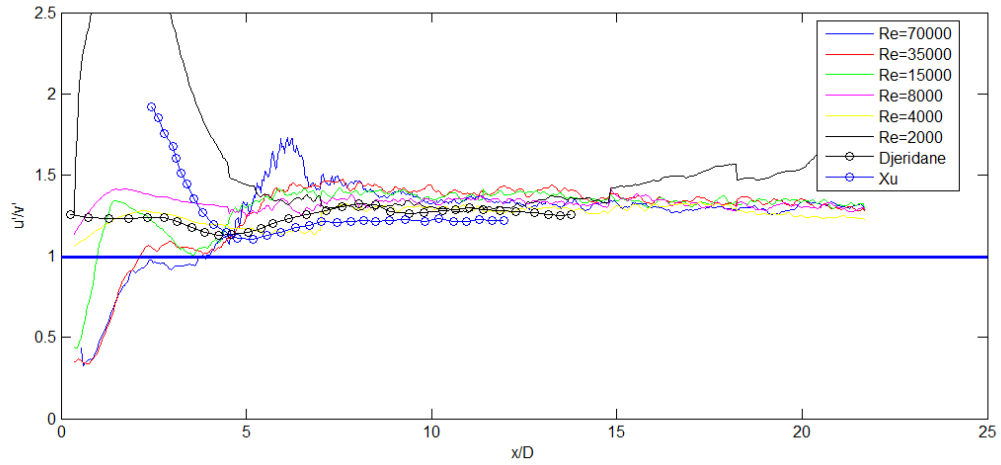

Figure 8. Centerline profile of the ratio u_{rms}/v_{rms} as measured at different Reynolds numbers. The black circles with dotted line refer to the data reported by Djeridane *et al.* (1996) [7], obtained on a circular pipe jet at a Reynolds number almost equal to 2×10^4, whereas the blue circles with dotted line to the data reported by Xu & Antonia (2002) [9] on a smooth contraction circular jet at Reynolds number equal to 8×10^4. The blue horizontal line refers to the exact isotropic conditions for the large scales.

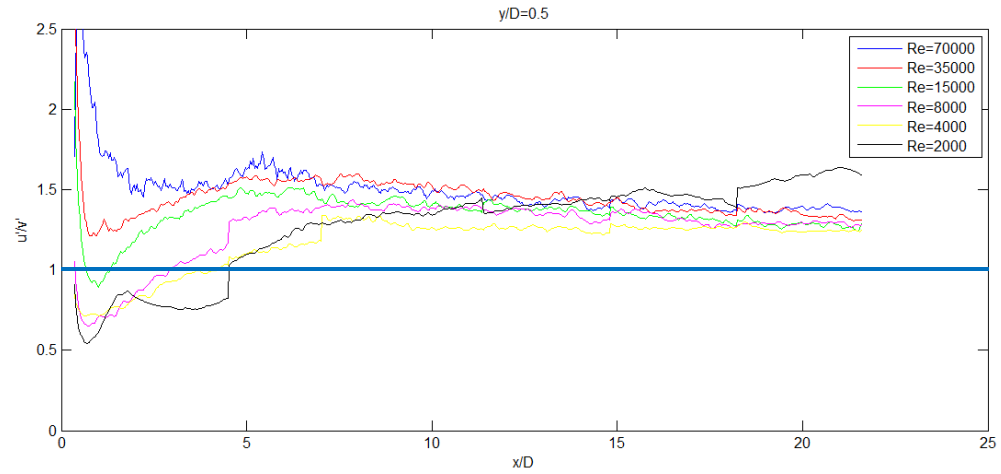

Figure 9. Profile of the ratio u_{rms}/v_{rms} as measured in the upper shear layer at different Reynolds numbers. The blue horizontal line refers to the exact isotropic conditions for the large scales.

Similarly, the u_{rms}/v_{rms} ratio can be computed in shear layers as reported in Figure 9 for the upper one. Again, except for the very small Reynolds number equal to 2000, the data are close one to each other for $x/D>7$ and approach an almost constant value which is the same as the one at the centreline, *i.e.* in the range (1.2 – 1.4) (similar results are obtained also for transverse profiles of this ratio, not shown here). Therefore, this confirms that the large scales, which dominate the *rms* ratio, are behaving not exactly as in isotropic conditions, with a significant departure from unity, being *rms* velocity fluctuations in the horizontal directions from 20% to 40% larger than those along the vertical. Nevertheless, this departure seems to be almost constant in the whole near field and almost independent of the specific Reynolds number, at least in the measured range. So far, as suggested in the Introduction, such an anisotropic behavior in the jet near field seems to be transported downstream by large scales all over the field and the question is how this is affecting also the small scale behavior.

3.2. Small scale statistics

The non-dimensional mean square derivatives, *i.e.* the ratios recalled in the Introduction of this paper, give an overall description of the small scale behavior in a flow field. In Figure10, examples of the four measured ratios in the near jet field are provided for a Reynolds number equal to 35,000. The largest values are usually measured beside the orifice, at the shear layer boundaries and sometimes in the jet core region and boundaries, being then convected and smoothed downstream. These values correspond to local high values of mean square velocity variations, either along the transverse direction (as for K_3 and K_1 respectively), in comparison to those in the streamwise direction (present in the normalization factor of the ratios, *i.e.* the average of $(\partial u'_1/\partial x_1)^2$), or due to the transverse velocity component (as in K_4) or the mixed ones (as in K_9) in comparison to the streamwise component alone. So, in some sense, these large values attest the importance of diffusion over transport processes for small scales. The isotropic values (respectively $K_1 = 1$, $K_3 = K_4 = 2$, $K_9 = -0.5$), correspond to blue and light blue colors in the previous color images and seem to be reasonably approached at this Reynolds number. However, a more detailed analysis related to this approximation and to Reynolds number dependence must be performed.

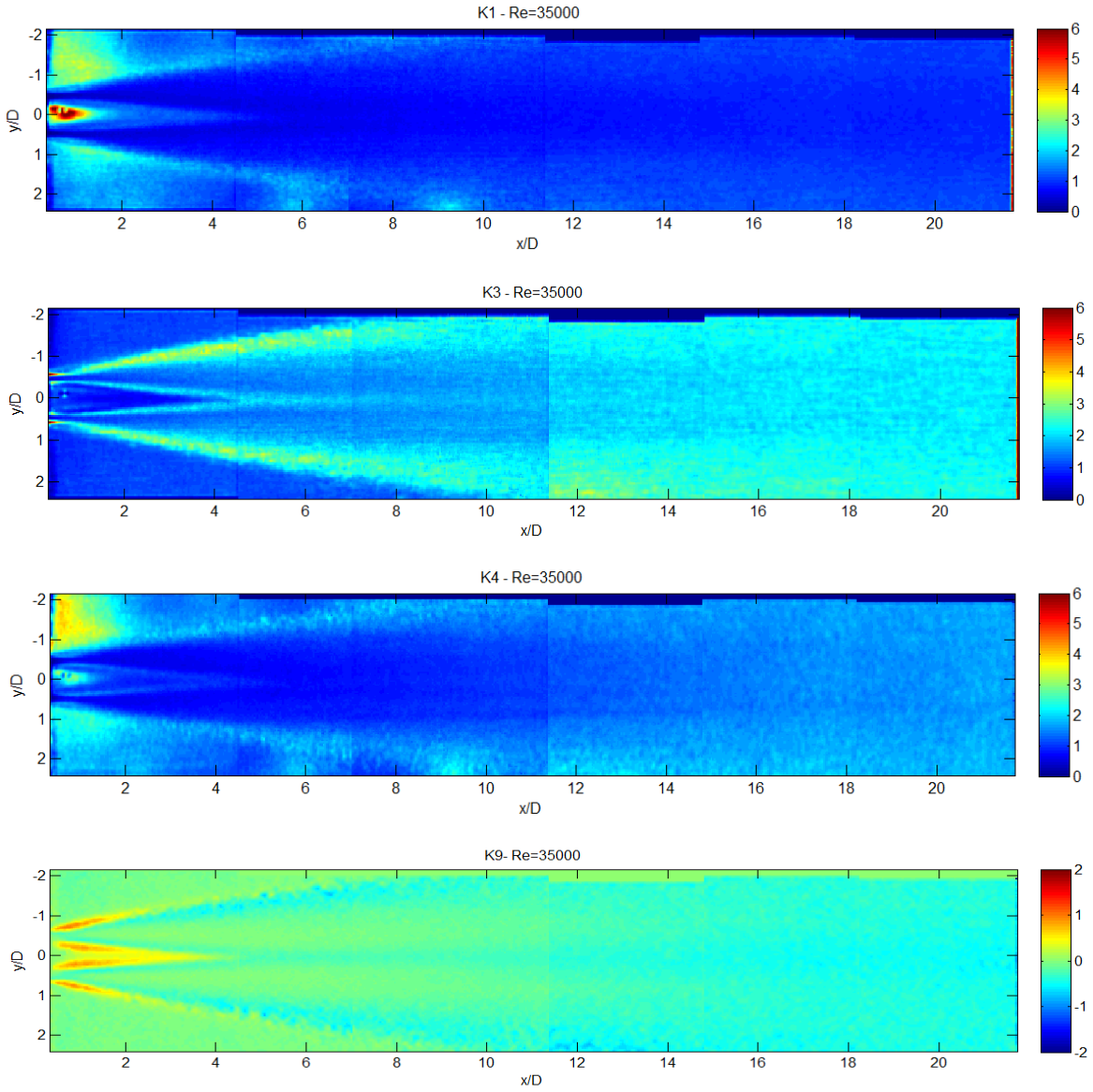

Figure 10. Colormaps of the four measured derivative ratios K_1, K_3, K_4, K_9 in the near field of the orifice jet for Reynolds number equal to 35,000. The flow direction is from left to right.

To this end, the behaviour of the four ratios is computed along the jet centreline at different Reynolds numbers and results are presented in Figure 11, together with the lines reproducing isotropic conditions. In agreement with results of other authors reported in the Introduction, the quantities K_1, K_3 and K_9 closely approach isotropy already for x/D=7, except possibly for a small deviation for the largest measured Reynolds number (Re=70,000), due to a slower convergence trend in comparison to smaller Reynolds numbers, due to the delayed jet development, already observed in Figures 3 and 4. On the other hand, for K_4, the deviation from the isotropic value is more pronounced and the isotropic value is not reached in the measuring range. As observed in Figure 10, this behavior is almost uniform all over the field, so that also in shear layers the quantity K_4 is still far to be equal to 2, as reported in Figure 12. The limiting value, which is approached as slowly as higher the Reynolds number, is quite similar to that along the centerline, *i.e.* within the interval (1.5 – 1.8).

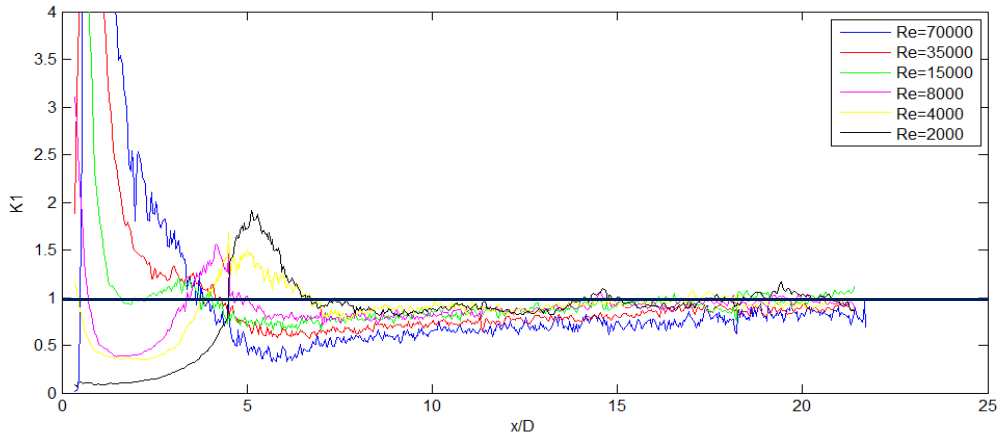

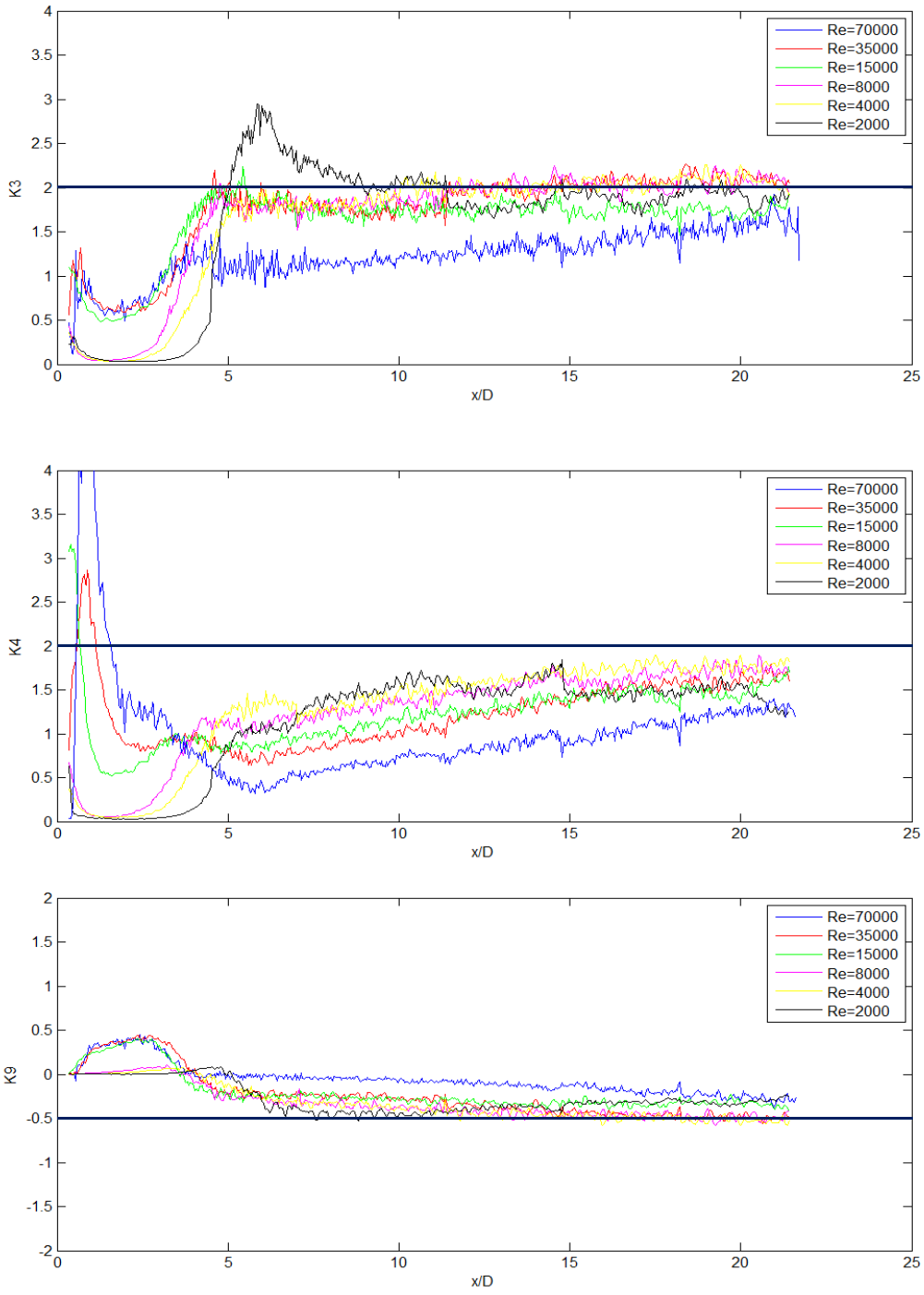

Figure 11. Centerline profile of the the four measured derivative ratios K_1, K_3, K_4, K_9 at different Reynolds numbers. The dark blue horizontal lines refer to the exact isotropic conditions for small scales.

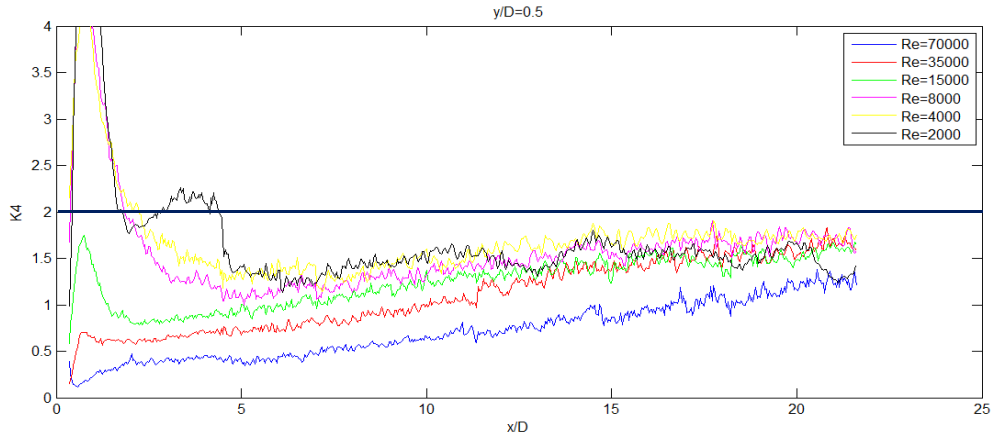

Figure 12. Profile of the derivative ratio K_4 as measured at the upper shear layer at different Reynolds numbers. The dark blue horizontal line refers to the exact isotropic conditions for the small scales.

3.3. Relation among large and small scales

As reported in the Introduction of this paper, relations among departure from isotropy conditions of small and large scales are derived. In this section, those relations are verified, by considering the direct measurements of the small scales ratios reported in the previous section (indicated for example as K_4 with the suffix "measured" in the following) and the computation of the same quantity as derived by the measurements of large scale ratios (indicated for example as K_4 with the suffix "computed" in the following). In Figure 13, such a comparison is presented for Reynolds number equal to 35,000 (similar behaviours are obtained for the other Reynolds numbers). Concerning the quantity K_4, the computed ratio, equal to $2R_1$, shows a behaviour very similar to the measured one, with high values beside the orifice, in shear layers and core regions, even if much more regular in comparison to the direct measurement, due to reduced errors in computing large rather than small scale statistics. The ratio among the computed over measured ratios is also presented in the last part of the figure, showing that an almost constant value is reached for $x/D > 7$ all over the measured field, even if this value seems to be slightly smaller than one (indicated as a factor A in the Introduction). This means that in

such a region, the computed value could represent a good approximation of the real ratio, being the factor A still to be determined precisely as also its dependence on Reynolds number.

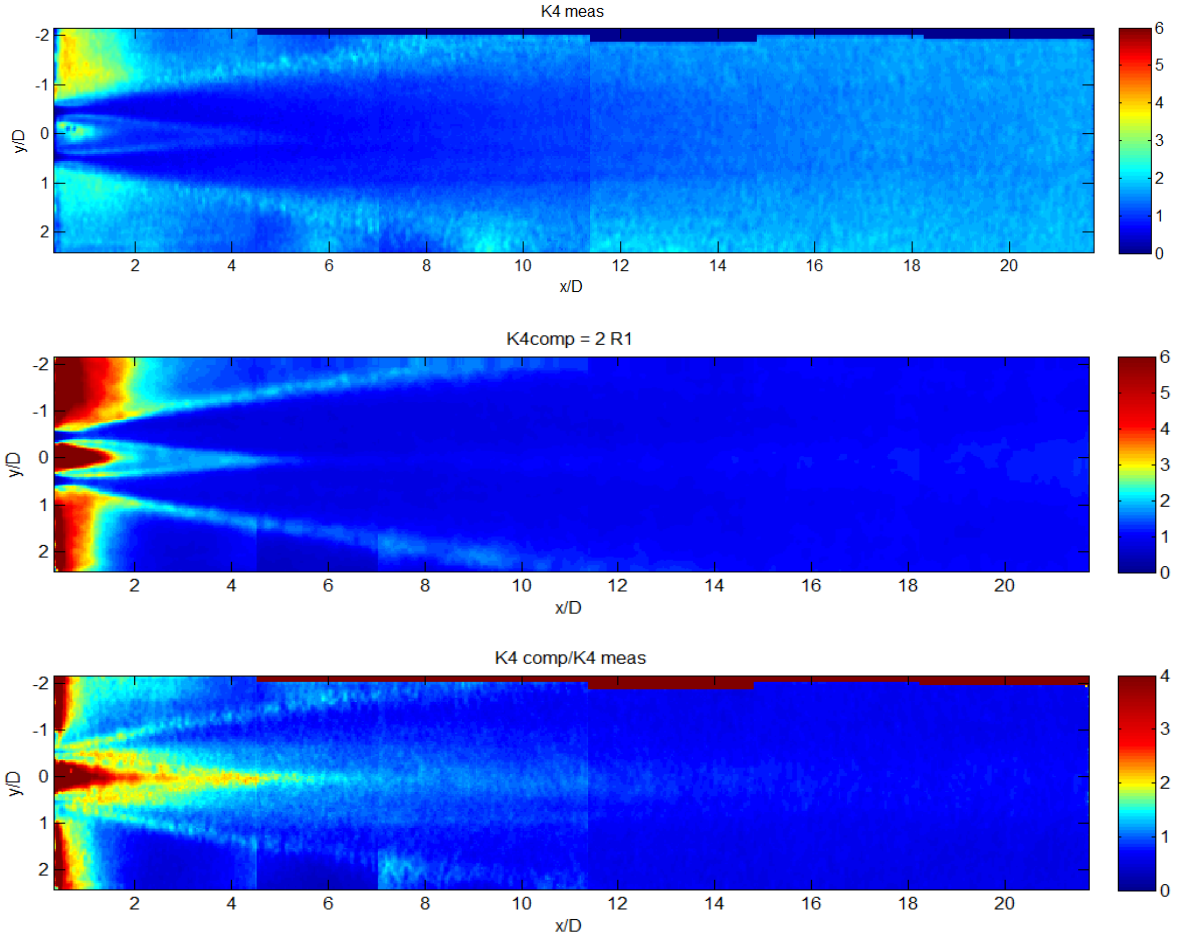

Figure 13. Colormaps of derivative ratio K_4 in the near field of the orifice jet for Reynolds number equal to 35,000. Direct measurement of the ratio, $K_{4\text{measured}}$, at the top, evaluation by the large scale ratio, $K_{4\text{computed}}=2R_1$, at the center, and ratio among the two at the bottom. The flow direction is from left to right.

Therefore, the ratio of K_4 "computed" over "measured" is investigated in detail in Figure 14, both at the centreline and in the shear layer, for the different Reynolds numbers tested in this work. For all data, there is a trend approaching a limiting constant value, except for those at the highest Reynolds number, still presenting a non-constant limiting behaviour, especially at the centreline, due to the already noticed slower approach as higher the Reynolds number. The asymptotic value, which is just the factor A, is very slightly dependent on Reynolds number and almost the same along the centreline and in the shear layer, being in the interval (0.6-0.8), of course in agreement with limiting value of the large scale ratio (given at the end of section 3.1) and of small scale ratio (given at the end of section 3.2).

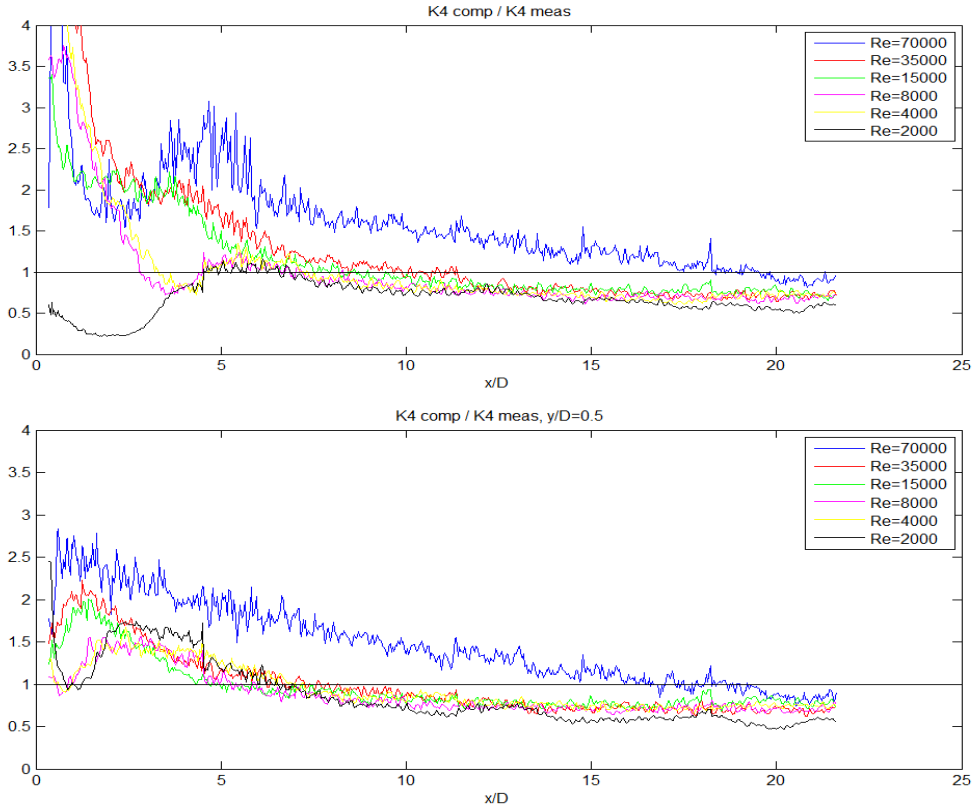

Figure 14. Profile of the ratio among computed and measured K_4, as measured at the centerline (at the top) and in the upper shear layer (at the bottom) at different Reynolds numbers. The horizontal lines refer to the perfect equivalence among computed and measured ratios.

Similarly, the ratio among K_3 and K_1 can be evaluated by the large scale computation equal to $2/R_1$, again multiplied by the same factor A as before. In Figure 15, the "measured", "computed" and the ratio among the two are shown for a Reynolds number equal to 35,000. Even if the overall behaviors of the directly measured and computed ratio seem to be very similar, the absolute values seem different. However, the observation of the ratio among the two, presented in the last figure, show an almost constant value, except for thin regions in shear layers and at the boundaries of the core region. As for the ratio K_4, presented before, the constant value is just the factor A, which seems to be smaller than one from the last plot. In order to derive detailed information on such a factor and on its dependence on Reynolds number, the "computed" over "measured" ratio is investigated in Figure 16, both at the centreline and in the shear layer, for the different Reynolds numbers tested. All data, approach a limiting constant value, which is just the factor A, already from $x/D \approx 6$, and this value is almost independent of Reynolds number and on the specific location, centreline or shear layer. The value is in the interval (0.5-0.7), in agreement with the one found previously, thus confirming the good verification of the proposed relation among isotropy indicators for large and small scales.

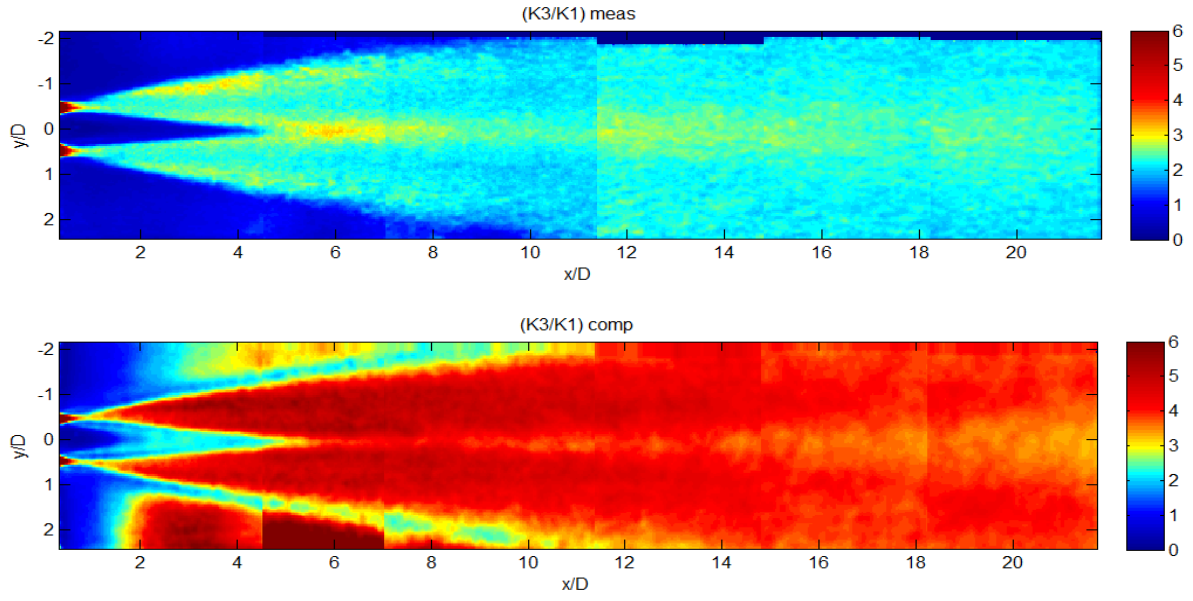

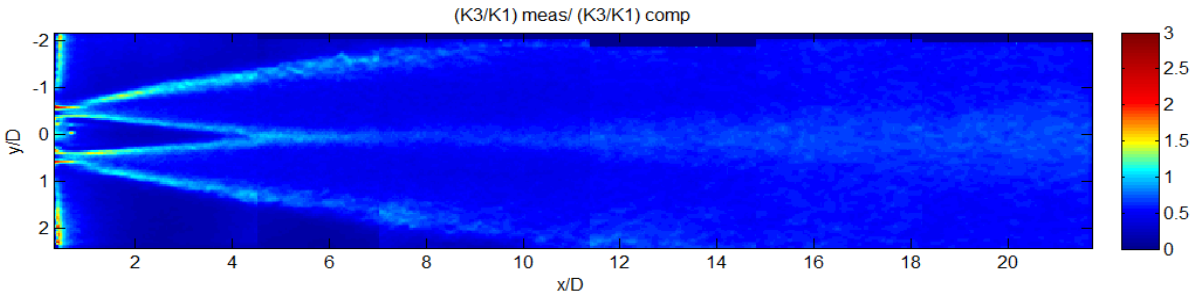

Figure 15. Colormaps of ratio K_3 /K_1 in the near field of the orifice jet for Reynolds number equal to 35,000. Direct measurement of the ratio, $(K_3/K_1)_{measured}$, at the top, evaluation by the large scale ratio, $(K_3/K_1)_{computed}$ $=2/R_1$, at the center, and ratio among the two at the bottom. The flow direction is from left to right.

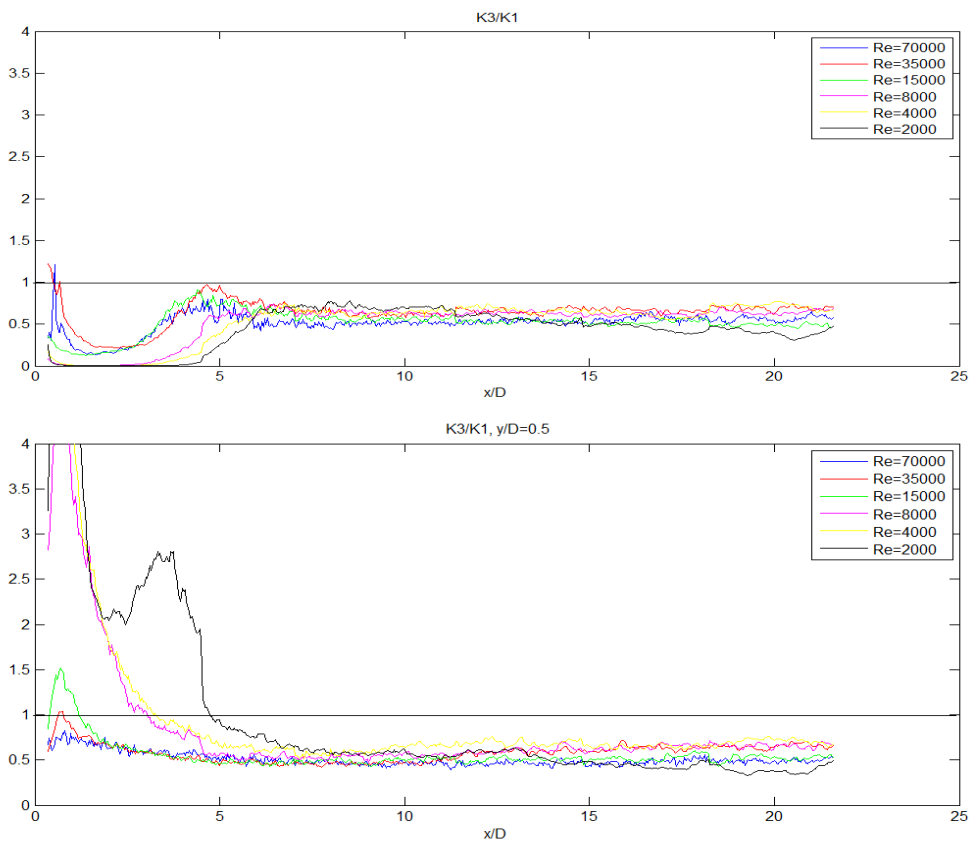

Figure 16. Profile of the ratio among computed and measured (K_3/K_1), as measured at the centerline (at the top) and in the upper shear layer (at the bottom) at different Reynolds numbers. The horizontal lines refer to the perfect equivalence among computed and measured ratios.

4. Remarks and Conclusions

The near field of a circular orifice turbulent jet is investigated experimentally in order to determine Reynolds number dependence and departures from isotropy for large and small scale statistics, with special focus onto velocity and velocity derivative mean square fluctuations. The required high spatial resolution for velocity derivative measurements is obtained by using Particle Image Velocimetry (PIV) in small partially overlapped sub-regions.

The large scale statistics is described in terms of mean velocity decay along the centerline and of the consequent jet half-width increase when moving along the streamwise direction, as derived by self-similarity hypotheses. For both those quantities, the observed behaviours are in agreement with results obtained by other authors, showing an initial decrease with Reynolds number (for Re<8000) of the velocity and width coefficients, K_U and K_S, followed by a plateau up to the maximum Reynolds number tested in this work (Re=70,000). This is shown in Figure 4 and indicates a sort of asymptotic scaling so that the behavior for all jets with Reynolds number larger than 10^4 could be considered as equivalent, at least for the mean field. No relevant modifications of the mean fields due to Reynolds number differences are observed, even very close to the jet orifice, *i.e.* in the core region ($x/D < 5$).

In addition, mean square velocity fluctuations have been obtained from data and are much more dependent on Reynolds number than the mean field for x/D<5. On the other hand, further from the jet exit, for both streamwise and vertical velocity components, there is a slight dependence on Reynolds number, especially noticed for the peak height at the centerline around $x/D \approx 7$, whereas almost no dependence for x/D>10. Thus, the ratio of streamwise to vertical mean square fluctuations is investigated and proved to be almost constant, (u_{rms}/v_{rms}) being in the range (1.2-1.4), and independent of Reynolds number for x/D>7, also in agreement with data by other authors, as shown in Figure 8. This value is constant all over the field, but significantly different from unity, this last being the prescribed value derived from the hypothesis of isotropy for the ratio $R_1=(v_{rms}/u_{rms})^2$. This last quantity is dominated by large scales, as derived by spectral contribution, so that a relevant departure from isotropy, equal for all Reynolds numbers, is observed for such large scales.

Mean square derivatives ratios are also computed in the measurement plane and compared at different Reynolds numbers, their spectral contribution deriving mainly from small scales. All measured ratios show asymptotic constant behaviours for x/D >10, almost independent of Reynolds number, even if the highest measured one is still showing an approaching trend in some ratios, as reported in Figure 11. For those ratios involving the transverse component, the transverse direction or both (as K_1, K_3, K_9), such asymptotic values are very close to what prescribed by the isotropy hypothesis (respectively equal to 1, 2, -0.5). On the other hand, for the ratio involving the streamwise direction (K_4) such asymptotic value is significantly different from 2, *i.e.* in the interval (1.5 – 1.8), even far from the centreline. It is reasonable to assume that this last ratio could be dominated by transport phenomena along the streamwise directions, whereas the other ratios should be more related to diffusion processes along the transverse direction. Starting form this point, it could be possible to relate the ratio K_4 to the large scale streamwise transport, *i.e.* to the ratio R_1 and this is just obtained in the Introduction of the paper under the additional hypothesis of incompressible flow.

Thus, the last part of the paper is devoted to the verification of the proposed relations and to the related dependency on Reynolds number. Except for the slower trend of the highest tested Reynolds number, which presumably will get the asymptotic value farther from the jet exit in comparison to smaller Reynolds numbers, all data indicate a constant factor to be included in the relation which is independent of Reynolds number. It is attained already for $x/D \approx 7$ and is constant all over the field with a value in the interval (0.5-0.8), as reported in Figures 14 and 16. These results verify the proposed relations and point out that the observed departures from isotropy of small scale are closely linked to departures from isotropy due to large scales, at least in the investigated turbulent jet flow and for the interval of Reynolds numbers tested in the present work. Therefore, it would be possible to derive the small scale derivative ratios, which are difficultly measured experimentally and numerically, due to high resolution requirements, from the determination of large scale ratios, which are obtained much easier and this could be very useful also for closure hypothesis.

Acknowledgements: The author thanks Giovanni Lacagnina for the help in data acquisition.

References

[1] G.K. Batchelor, The theory of axisymmetric turbulence, Proc. R. Soc. Lond. A 186 (1946) 480–502.

[2] W.K. George, H.J. Hussein, Locally axisymmetric turbulence, J. Fluid Mech. 233 (1991) 1–23.

[3] A.S. Monin, A.M. Yaglom, Statistical fluid mechanics, M.I.T. Press, Cambridge, Mass., 1971.

[4] H. Tennekes, J.L. Lumley, A first course in turbulence, M.I.T. Press, Cambridge, Mass., 1972.

[5] G.I. Taylor, GI (1935) Statistical theory of turbulence, Proc. R. Soc. Lond, A 151(873) (1935) 421–444.

[6] G. Lacagnina, G.P. Romano, PIV investigations on optical magnification and small scales in the near-field of an orifice jet, Exp. Fluids 56 (2015) 5.

[7] T. Djeridane, H. Amielh, F. Anselmet, F. Fulachier, Velocity turbulence properties in the near-field region of axisymmetric variable density jets, Phys. Fluids 8(6) (1996) 1614–1630.

[8] B.J. Boersma, G. Brethouwer, F.T.M. Nieuwstadt, A numerical investigation on the effect of the inflow conditions on the self-similar region of a round jet, Phys. Fluids 10 (1998) 899-909.

[9] G. Xu, R.A. Antonia, Effect of different initial conditions on a turbulent round free jet, Exp. Fluids 33 (2002) 677–683.

[10] J. Mi, P. Kalt, G.J. Nathan , C.Y. Wong, PIV measurements of a turbulent jet issuing from round sharp-edged plate, Exp. Fluids 42 (2007) 625–637.

[11] C. Bogey, C. Bailly, Turbulence and energy budget in a self-preserving round jet: direct evaluation using large eddy simulation, J. Fluid Mech. 627 (2009) 129–160.

[12] G.P. Romano, M. Falchi, Recovering isotropy in turbulent jets. In: 8*th* Int. ERCOFTAC Symposium on Engineering Turbulence Modelling and Measurements, Marseille, France (2010).

[13] F. Shan, A. Fujishiro, T. Tsuneyoshi, Y. Tsuji, Particle image velocimetry measurements of flow field behind a circular square-edged orifice in a round pipe, Exp. Fluids 54 (2013) 1553.

[14] A.P. Vouros, Panidis Th., Turbulent properties of a low Reynolds number, axisymmetric, pipe jet, Exp. Thermal and Fluid Science 44 (2013) 42–50.

[15] A. Hashiehbaf, G.P. Romano, Particle image velocimetry investigation on mixing enhancement of non-circular sharp edge nozzles, Int. Journal of Heat and Fluid Flow 44 (2013) 208–221

[16] J.O. Hinze Turbulence, McGraw-Hill, 1975.

[17] G.P. Romano, Chapter C10.1 - Springer Handbook of Experimental Fluid Mechanics, Edited by C. Tropea, A. L. Yarin, J. F. Foss, Springer, 2007.

[18] M. Stanislas, K. Okamoto, C.J. Kahler, J. Westerweel, F. Scarano F, Main results of the third International PIV Challenge. Exp. Fluids, 45, (2008), 27-71.

[19] R.A. Antonia, Y. Zhu, J. Kim, On the measurement of lateral velocity derivatives in turbulent flows, Exp. Fluids 15 (1993), 65-69.

[20] A. Hashiehbaf, G.P. Romano, An experimental investigation on mixing enhancements in non-circular sharp-edged nozzles using the entropy production concept, Journal of Turbulence 15, 7 (2014) 421–428.

[21] W.R. Quinn, Experimental study of the near field and transition region of a free jet issuing from a sharp-edged elliptic orifice plate, Eur. J. Mech., B: Fluids 26 (2007) 583–614.

[22] W.R. Quinn On mixing in an elliptic turbulent free jet, Phys Fluids 1(10) (1989) 1716–1722.

[23] I. Wygnanski, H. Fiedler, Some measurements in the self-preserving jet, Journal of Fluid Mech. 38-3 (1969) 577-612.

[24] W.R. Quinn, Upstream nozzle shaping effects on near field flow in round turbulent free jets, Eur. J. Mech., B: Fluids 25 (2006) 279–301.

[25] C.J. Chen, W. Rodi, Vertical Turbulent Buoyant Jets a Review of Experimental Data, Pergamon Press, 1980.

[26] N.R. Panchapasekan, J.L. Lumley, Turbulence measurements in axisymmetric jets of air and helium. Part 1: Air Jet, J. Fluid Mech. 246 (1993) 197–223.